soil systems

MDPI

Article

Investigating Lead Bioavailability in a Former Shooting Range by Soil Microanalyses and Earthworms Tests

Carlo Porfido [1,*], Concetta Eliana Gattullo [1], Ignazio Allegretta [1], Nunzio Fiorentino [2], Roberto Terzano [1], Massimo Fagnano [2] and Matteo Spagnuolo [1]

[1] Dipartimento di Scienze del Suolo, Della Pianta e Degli Alimenti, Università Degli Studi di Bari "Aldo Moro", Via Amendola 165/A, 70126 Bari, Italy; concettaeliana.gattullo@uniba.it (C.E.G.); ignazio.allegretta@uniba.it (I.A.); roberto.terzano@uniba.it (R.T.); matteo.spagnuolo@uniba.it (M.S.)

[2] Dipartimento di Agraria, Università Degli Studi di Napoli "Federico II", Via Università 100, 80055 Portici, Italy; nunzio.fiorentino@unina.it (N.F.); massimo.fagnano@unina.it (M.F.)

* Correspondence: carlo.porfido@uniba.it

Abstract: Shooting ranges are among the major anthropogenic sources of Pb contamination in soils worldwide. Once they have reached the soil, bullet residues can have different fates according to the characteristics of the soil environment, leading to the formation of different Pb weathering products whose stability is crucial for Pb accessibility to soil biota. In this study, Pb availability in a former polluted shooting range was investigated with a combination of conventional soil analyses, X-ray microanalyses and assays with the bio-indicator earthworm *Eisenia andrei*. Chemical extractions evidenced a rather low mobility of soil Pb, while micro-X-ray fluorescence spectroscopy (μXRF) and scanning electron microscopy coupled with microanalysis (SEM-EDX) showed the formation of a weathering crust around Pb-containing bullet slivers dispersed within the soil. Such crusts consisted of a mixture of orthophosphates, including the highly insoluble Cl-pyromorphite. Furthermore, no acute toxicity effects and low Pb concentration values were measured in earthworm tissues (94.9 mg kg^{-1}) and coelom fluids (794 μg L^{-1}) after 28 days of exposure to the polluted soil. These results allow us to assume that most of the Pb in the shooting range soil underwent stabilization processes promoted by phosphatic fertilization. The soil was in fact used for agriculture after being dismissed for firing activities. Such a combined approach can be applied to study Pb bioavailability in other shooting ranges or, more generally, in soils heavily polluted with Pb.

Keywords: firing ranges; *Eisenia andrei*; micro-X-ray fluorescence; SEM-EDX; Pb phosphates; pyromorphite

Citation: Porfido, C.; Gattullo, C.E.; Allegretta, I.; Fiorentino, N.; Terzano, R.; Fagnano, M.; Spagnuolo, M. Investigating Lead Bioavailability in a Former Shooting Range by Soil Microanalyses and Earthworms Tests. *Soil Syst.* **2022**, *6*, 25. https://doi.org/10.3390/soilsystems6010025

Academic Editor: Mallavarapu Megharaj

Received: 11 February 2022
Accepted: 10 March 2022
Published: 13 March 2022

1. Introduction

Lead (Pb) is a non-essential and non-beneficial element whose average content in uncontaminated soils worldwide is estimated to equal 17 mg kg^{-1} [1]. However, anthropogenic sources, such as mining and smelting, shooting ranges, automobile exhausts and sewage sludges, can cause Pb contamination in quantities up to several thousand mg kg^{-1} with huge risks for the environment and human beings. For instance, exposure to Pb-contaminated soil and ingestion of soil Pb-bearing particles and dusts has been indicated as the major pathway for Pb poisoning in children, which can pose risks for cognitive development and various diseases [2]. Despite Pb being quite stable in soils due to strong complexation or adsorption by humic substances, clay minerals and Fe oxides [1], plants and other soil inhabitants can suffer from Pb exposure, with lethal effects [3–5]. Pb can accumulate in their tissues and thereby be transferred to higher levels of the trophic chain [6].

In recent years, various studies have demonstrated the advantages of laboratory and synchrotron micro-X-ray florescence (μXRF) and hyperspectral elaboration of μXRF data in investigating the distribution and speciation of potentially toxic elements (PTEs) in polluted

soils [7–14]. Indeed, through the assessment of element distributions in soil thin sections and their mutual correlations it is possible to infer, for instance, chemical speciation and mineralogical information, which are crucial especially for those (minor) phases otherwise not detectable with other techniques (e.g., X-ray diffraction) due to their weak abundance and/or crystallinity. Such outcomes can be further combined with more detailed observations at the sub-micrometric scale by means of scanning electron microscopy coupled with microanalysis (SEM-EDX), which additionally allows the detection of light elements not observable by μXRF. However, if, on the one hand, soil microanalysis offers an effective tool for predicting PTE behaviour and mobility based on chemical speciation or associations with soil phases, on the other hand, the use of bio-indicator species allows the appraisal of the actual impact of the pollutant on soil organisms. For decades, earthworms have been elected as the favoured bio-indicators in soils because of their peculiar living and feeding mode. Indeed, they are intimately exposed to soil-bound contaminants through integument contact and ingestion [15]. Moreover, earthworms accumulate pollutants in their bodies at higher rates than other soil organisms [16,17]. The combination of soil microanalysis and earthworm bioassays can therefore be used to evaluate the occurrence and speciation of PTEs in soil as well as their bioaccessibility.

In the present study, Pb bioavailability in a polluted soil (1575 mg Pb kg^{-1}) from a former shooting range area (Acerra, Italy) was studied using a synergistic approach combining: (a) physicochemical characterization through conventional analytical methods; (b) soil microanalysis by μXRF and SEM-EDX observations; (c) toxicological tests using earthworms *Eisenia andrei* Bouché. The outcomes obtained from this research could be useful in assessing the actual environmental risks of Pb contamination in the area under investigation as well as devising possible remediation strategies.

2. Materials and Methods

2.1. Soil Sampling and Physicochemical Characterization

The polluted soil (S2) was collected at the former shooting range of Acerra (40°59′37.74″ N; 14°24′7.27″ E), district of Naples, Southern Italy. The shooting range covered an area of approximately 6 ha and was dismissed in 2003 after about 10 years of activity. Once abandoned, the site has been colonized by spontaneous vegetation and then used for agricultural production from 2011 to 2014 and finally confiscated by Regional Authorities. In 2019 the site was assigned to the University of Naples for developing a phytoremediation project as part of the activities of the Rizobiorem project. A huge amount of bullet residues, mainly in the form of metallic slivers, was dispersed in the ground, featuring levels of Pb, Sb and polycyclic aromatic hydrocarbons (PAH) exceeding the national regulatory thresholds for agricultural sites (Ministerial Decree n. 46/2019) [18]. An agricultural uncontaminated soil (S1) in the close vicinity of the shooting area was sampled and used as a reference control soil. Both S1 and S2 were collected (2019) in three replicates at 0–20 cm soil layer after removing the very superficial undecomposed litter. Soil samples were air-dried and sieved through a 2 mm mesh.

The soil physicochemical characterization included the following parameters: particle size distribution (pipette and sieving method) [19]; electrical conductivity (1:5 soil:water solution ratio) [20]; pH H_2O (1:2.5 soil:water solution ratio, pH meter GLP 22, Crison ^{TM}); calcium carbonate (titrimetric method [21]); total nitrogen (Kjeldahl); available phosphorous (Olsen); and organic carbon (Walkley and Black) [22]. Furthermore, the promptly bioavailable fraction of PTEs was estimated by ammonium nitrate extraction [23,24] and the pseudototal PTE contents were quantified by aqua regia digestion (ISO 12914) and ICP-MS (PerkinElmer Nexion 300, Waltham, MA, USA) [25,26]. Pseudototal PTE content was compared to screening values (SV) reported in Italian M.D. 46/2019.

Soil main minerals were determined by means of X-ray powder diffraction (XRPD) using a Miniflex II X-ray diffractometer (Rigaku Corporation, Tokyo, Japan) equipped with a Cu tube (Cu Kα, 30 kV, 15 mA). Data were acquired between 3 and 70° 2θ with a step width of 0.02° 2θ and a counting time of 3 s/step.

2.2. Soil μXRF and SEM EDX Analyses

Petrographic soil thin sections (30 μm thickness) of both control and polluted soils were prepared after embedding the soils in epoxy resin (L.R. White Resin, Polyscience Europe GmbH, Hirschberg an der Bergstrasse, Germany) [7] and were analysed with a micro-X-ray fluorescence spectrometer (μXRF, M4 Tornado, Bruker Nano GmbH, Berlin, Germany). Elemental distribution maps were acquired under vacuum (20 mbar) using a Rh tube X-ray source (50 kV, 600 μA, 30 W, spot size of 25 μm) with policapillary optics and two 30 mm^2 XFlash® silicon drift detectors. Micro-X-ray maps were collected with a step size of 25 μm and an acquisition time of 10 ms per pixel. Details of Pb slivers were acquired with a smaller step size (5 μm) and by repeating the scanning 5 times to increase the signal-to-noise (S/N) ratio. X-ray fluorescence hyperspectral data were processed using both Bruker M4 software and a combination of PyMca 5.1.3 (Copyright (c) 2004–2019 European Synchrotron Radiation Facility (ESRF), Grenoble, France) [27] and Datamuncher software [28] in order to evaluate both element distribution and correlations. Furthermore, a field emission gun (FEG) SEM Zeiss Σigma 300 VP (Zeiss Oberkochen, Oberkochen, Germany) was used to observe the samples with a sub-micrometric resolution. The instrument, working at 15 kV, was equipped with an energy-dispersive spectrometer (EDX) C-MaxN SDD with an active area of 20 mm^2 (Oxford Instruments, Oxford, UK).

2.3. Earthworm Testing and Analysis

Soil mesocosms of S1 and S2 were prepared in triplicate using plastic boxes containing approximately 500 g of soil (dry weight, sieved at 2 mm), following the OECD guidelines [29]. Ten mature (clitellate) earthworms of *E. andrei* (provided by our laboratory stockbreeding) of about 350−400 mg individual weight were introduced into each mesocosm after 24 h of gut depuration in Petri dishes (in the dark at 22 ± 2 °C). The mesocosms were then placed in an incubator chamber (21 ± 1 °C, 65 ± 5% RH) for 28 days, adjusting the moisture content when required. Finally, the earthworms were recovered, cleaned, purged for 48 h (in Petri dishes on a wet filter paper), rinsed with deionized water and weighed. Five specimens per mesocosm were used for tissue bioaccumulation analyses, while the other five individuals were used for coelom fluid extrusion and analysis. Lead concentration in earthworm tissues and in the coelom fluid were determined using a total reflection X-ray fluorescence spectrometer (S2 Picofox—Bruker Nano GmbH, Berlin, Germany) equipped with a Mo microfocus tube (30 W, 50 kV, 600 μA), a multilayer monochromator and a XFlash SDD with a 30 mm^2 active area. For Pb determination in tissues, samples were dried (48 h, 50 °C) and finely ground using a mixer mill (MM 400, Retsch GmbH, Haan, Germany). Then, suspensions were prepared, with 50 mg of each specimen placed in a 15 mL polypropylene centrifuge tube to which 2.5 mL of Triton X-100 (Sigma-Aldrich, Darmstadt, Germany) was added along with 10 μL of a 1000 μg L^{-1} yttrium (Y) standard solution (Sigma-Aldrich) as internal standard (IS). Coelom fluids were extruded, applying a voltage of 5 V for 3 s to each earthworm. Then, 10 μL of the extruded fluid was mixed with 80 μL of polyvinyl alcohol (PVA) and 10 μL of Y standard solution, as IS. All samples were analysed for 1000 s (live time) following the method described in [30,31]. The average weight of the earthworms before and after the testing period was calculated by dividing the mass of all earthworms by their number for both S1 and S2 mesocosms. The bioconcentration factor (BF) was calculated by dividing tissue mean Pb concentration by total Pb concentration in the soil.

3. Results and Discussion

3.1. Soil Main Properties

Soil physicochemical properties for both S1 and S2 are reported in Table 1. Both S1 and S2 were sandy loam soils with slightly alkaline pH according to USDA classification [32]. The organic matter (OM) content was higher in S2 (53 g kg^{-1}) than in S1 (31 g kg^{-1}). In addition, the available P was higher in S2 (P_2O_5 = 0.60 g kg^{-1}), almost double that of S1. As

for the total carbonate content, S1 was highly calcareous and S2 was moderately calcareous. Both soils were non-saline according to their EC values.

Table 1. Physicochemical properties of the unpolluted (S1) and polluted (S2) soils.

	Sand	Silt $g\ kg^{-1}$	Clay	pH (H_2O)	EC $dS\ m^{-1}$	OC [a] $g\ kg^{-1}$	OM [b] $g\ kg^{-1}$	N $g\ kg^{-1}$	C/N	$CaCO_3$ $g\ kg^{-1}$	P_2O_5 $g\ kg^{-1}$
S1	600	240	160	7.8	0.21	18	31	2.2	8	155	0.29
S2	590	265	145	7.4	0.21	30	53	2.5	12	70	0.60
	Cd $mg\ kg^{-1}$	**Sb** $mg\ kg^{-1}$	**Pb** $mg\ kg^{-1}$	**Zn** $mg\ kg^{-1}$	**Cd** * $mg\ kg^{-1}$	**Sb** * $mg\ kg^{-1}$	**Pb** * $mg\ kg^{-1}$	**Zn** * $mg\ kg^{-1}$			
S1	0.3	0.3	17	209	0.03	0.61	0.01	0.3			
S2	3.3	22.7	1575	328	0.15	6.36	0.02	1.3			
SV	5	10	100	300	n.a.	n.a.	n.a.	n.a.			

[a] Organic carbon. [b] Organic matter. * NH_4NO_3 extractable. SV screening value M.D. n. 46/2019; n.a.: not available.

The soils showed similar mineralogy, the main minerals detected being silicates and aluminium silicates, such as quartz, feldspars, albite and illite/muscovite. The presence of calcite and apatite group minerals was also observed. No Pb-bearing phases were detected by XRPD. The concentrations of Sb, Pb and Zn in S2 were higher than the national screening values (SV) for agricultural soil [18]; in particular, Pb concentration was 1575 mg kg^{-1} compared to a SV of 100 mg kg^{-1}.

3.2. Soil Microanalysis

Micro-XRF was used to map and compare elemental distributions in soil thin sections of both the control and the polluted soil (Figure 1). The major elements, e.g., Al, Si, P, S, K, Ca and Fe, occurred with similar abundances and correlations in the two soils and could be attributed to the soil mineral constituents. Based on XRPD analysis, the overlapping distribution of Al, Si and K testifies to the presence of aluminium silicates, while the dark blue Si-containing particles in Figure 1 (middle panels) are instead related to quartz grains. Calcium is mainly associated with P (purple particles, Figure 1, right panels), presumably forming calcium phosphate phases, such as apatite; in other particles, Ca occurs uncorrelated with other elements, hence it is likely attributable to calcite (pure red particles, Figure 1, right panels), since C and O cannot be detected by XRF.

As expected, Pb was detected only in the polluted soil (S2), concentrated in particles ranging in size from hundreds to thousands of microns, visible as green areas (Figure 1b, right). Except for P, no other element was correlated with Pb. Several Pb-containing particles were then selected on the PTE-polluted soil thin sections and analysed again with increased resolution and accuracy in order to better investigate the nature of these Pb-containing particles as well as Pb vs. P correlations.

In Figure 2, the results of the μXRF hyperspectral data analysis performed on three Pb-containing particles, selected as the most representative, are shown. For each particle, the optical image is coupled with its false-colour map, which depicts the correlation between Pb and P fluorescent signals detected at the particle section surface.

From the scatterplot of the intensities (expressed as counts) of the Pb L-lines and P Kα-lines recorded in each pixel of the three micrographs shown in Figure 2, five main P/Pb correlations were identified and grouped with different colours (Figure 2a). The green region of the scatterplot contains those pixels containing almost only Pb, while the yellow, magenta, red and blue regions contain those pixels with an increasingly higher content of P, beside Pb. By applying such colour-based segmentation to the Pb-particle micrographs (Figure 2b–d, right), it can be generally observed that, starting from the inner only-Pb-containing core (green areas of the particles), the P amount gradually increases towards the particle boundaries, with the higher P/Pb signal ratio (blue) observed at the border of the particle. Such a pattern is clearly visible for the particle shown in Figure 2c (right), while such distribution is slightly more structured in the other particles (Figure 2b,d, right).

This depends on the particles shape and on the cutting section, which was reasonably diametrical for particle (c) and more external for the others. By looking at the composition of the particles and at their morphology with a light microscope, they appear as metallic Pb slivers deriving from bullet residues. Indeed, many bullet residues are still present in the investigated soils. Furthermore, the comparison between the correlation maps and their corresponding light micrographs (Figure 2b–d, left) shows other additional interesting features: in the case of Figure 2c, for instance, the sliver shows a Pb-rich nucleus (sliver core) which appears pale in visible light, becoming darker as the P/Pb ratio increases moving toward the borders of the particle.

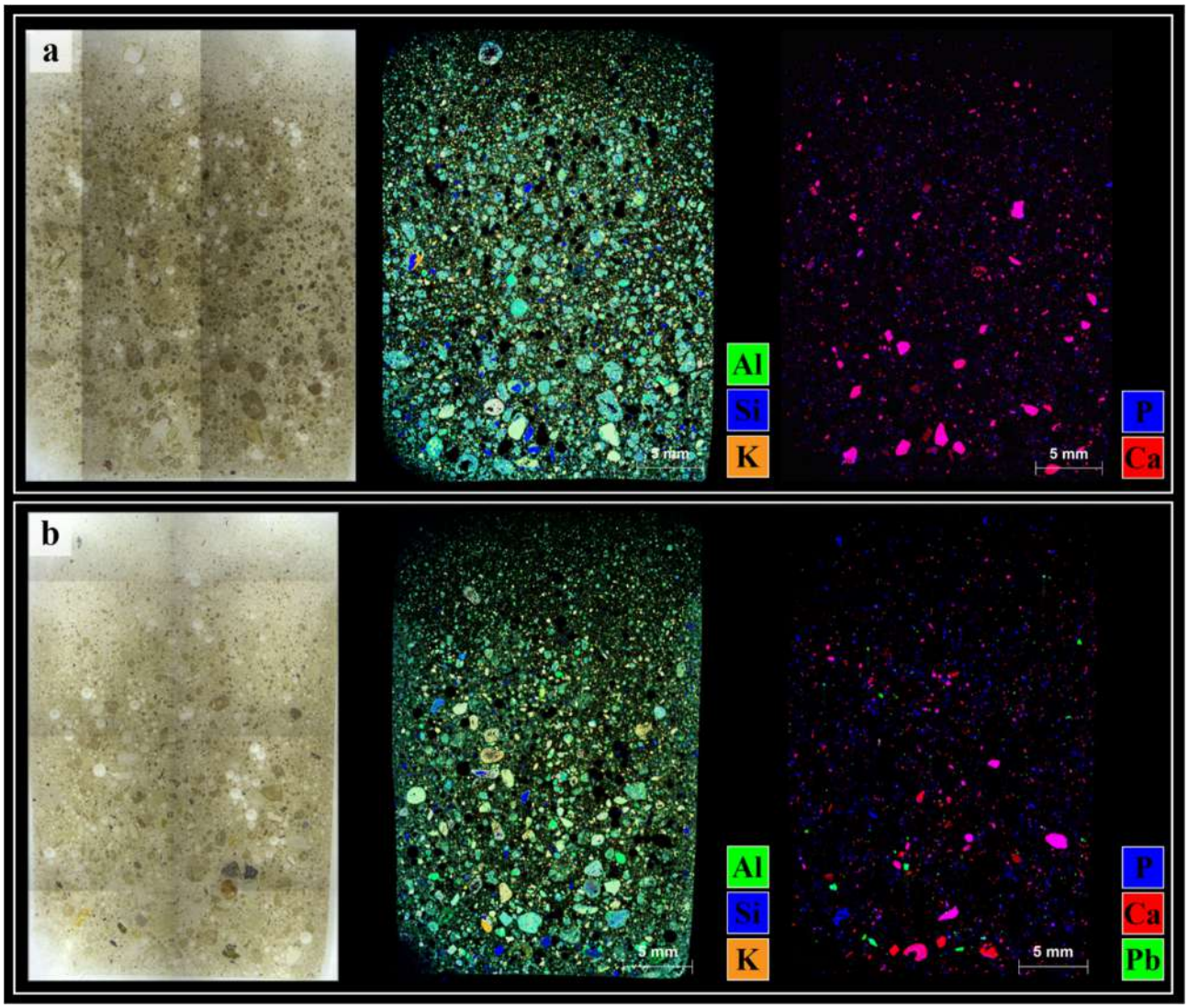

Figure 1. Thin section images (left) and corresponding μXRF maps (middle, right) of S1 (**a**) and S2 (**b**) soils. ((**a**,**b**) middle panels) Overlay of Al (green), Si (blue) and K (orange) distribution maps. ((**a**,**b**) right panels) Overlay of P (blue), Ca (red) and Pb (green) distribution maps. Brighter pixels correspond to higher element concentrations. The co-presence of two or more elements in the same pixels gives rise to different degrees of colour combinations.

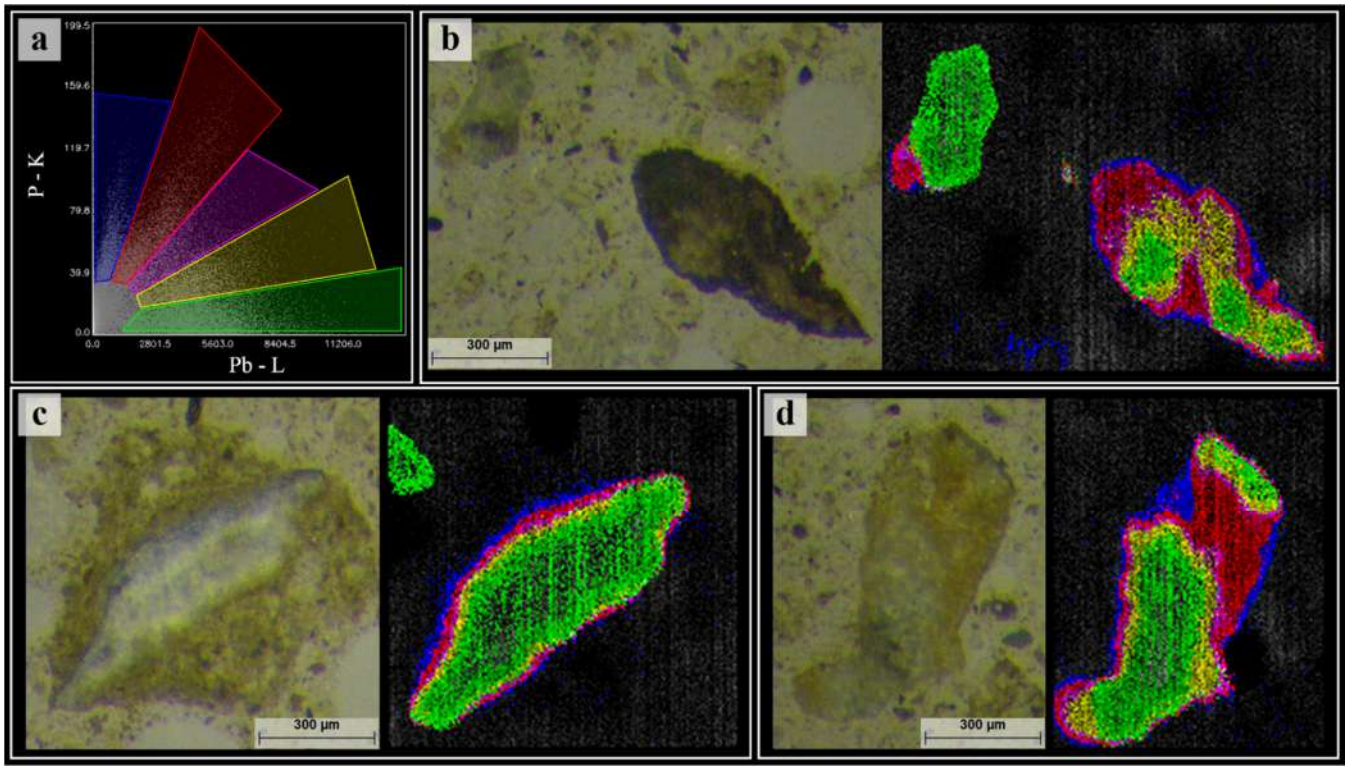

Figure 2. (**a**) P (K fluorescent signal) vs. Pb (L fluorescent signal) scatterplot obtained using spectral µXRF deconvolution data of (**b**–**d**) particles. (**b**–**d**) particles micrographs (**left**) and related correlation maps (**right**) coloured according to the different P/Pb correlations identified through the scatterplot (**a**)).

Other interesting correlations observed after spectral deconvolution are those between Cl and P and between Ca and P, shown in the scatterplots in Figure 3a,c. Although with low intensity, the Cl–K signal is correlated with that of P (Figure 3a) and is not detected where only the Pb signal is present (without P; grey regions in Figure 3b). Chlorine is located only in the portions of the particles where P was also detected. The scatterplot in Figure 3c instead shows three main Ca–P correlations grouping pixels whose Ca content is yellow < green < red. By looking at the corresponding false-color micrographs (Figure 3d), the primary evidence is that such Ca–P correlations occur in the same pixels where also P–Pb and Cl–P correlations were observed. Moreover, it can be noticed that the higher Ca intensities are located at the very external borders of the Pb-containing particles whilst they decrease as they move towards the inner part (green > yellow).

Beside P, Ca and Cl, no other chemical element has been detected within these Pb-containing fragments. The ubiquitous occurrence of P and Ca should indicate the presence of Ca phosphates (or even Cl apatite), while the presence of P and Cl, together with Pb should be attributed to the formation of Pb phosphates over the metallic slivers, such as secondary and tertiary Pb phosphates (Pb_2HPO_4 and $Pb_3(PO_4)_2$, respectively) and/or pyromorphite. The latter refers to three species, depending on the anion X in the structure $Pb_5(PO_4)_3X$ (namely, chloropyromorphite, where X = Cl^-; hydroxypyromorphite, where X = OH^-; and fluoropyromophite, where X = F^-). Unfortunately, neither F nor O and H can be detected by µXRF, therefore none of these three forms can be excluded, chloropyromorphite most likely being present.

Lead orthophosphates, above all pyromorphite, are highly insoluble phases. In 1932, Jowett and Price [33] determined an extremely low solubility product (K_{sp}) of $10^{-79.115}$ for $Pb_5(PO_4)_3Cl$, which is the most insoluble Pb orthophosphate known. In the same study, the authors demonstrated that secondary and tertiary orthophosphates transform to pyromorphite even in the presence of low chloride concentrations, thus explaining the fact that, while the first two phases are not found in nature, pyromorphite is rather common.

Subsequent studies [34,35] proposed for $Pb_5(PO_4)_3Cl$ the K_{sp} of $10^{-25.05}$ for soil with a pH in the usual range. However, even considering the higher value of $10^{-25.05}$, pyromorphite can be still considered several orders of magnitude less soluble than the most common Pb minerals in soils [2]. Indeed, the use of phosphates for amending Pb-polluted soils is a well-known and common remediation practice. By promoting the formation of Pb insoluble species, such as pyromorphite, phosphate addition leads to the reduction of Pb bioavailability and toxicity [2,36].

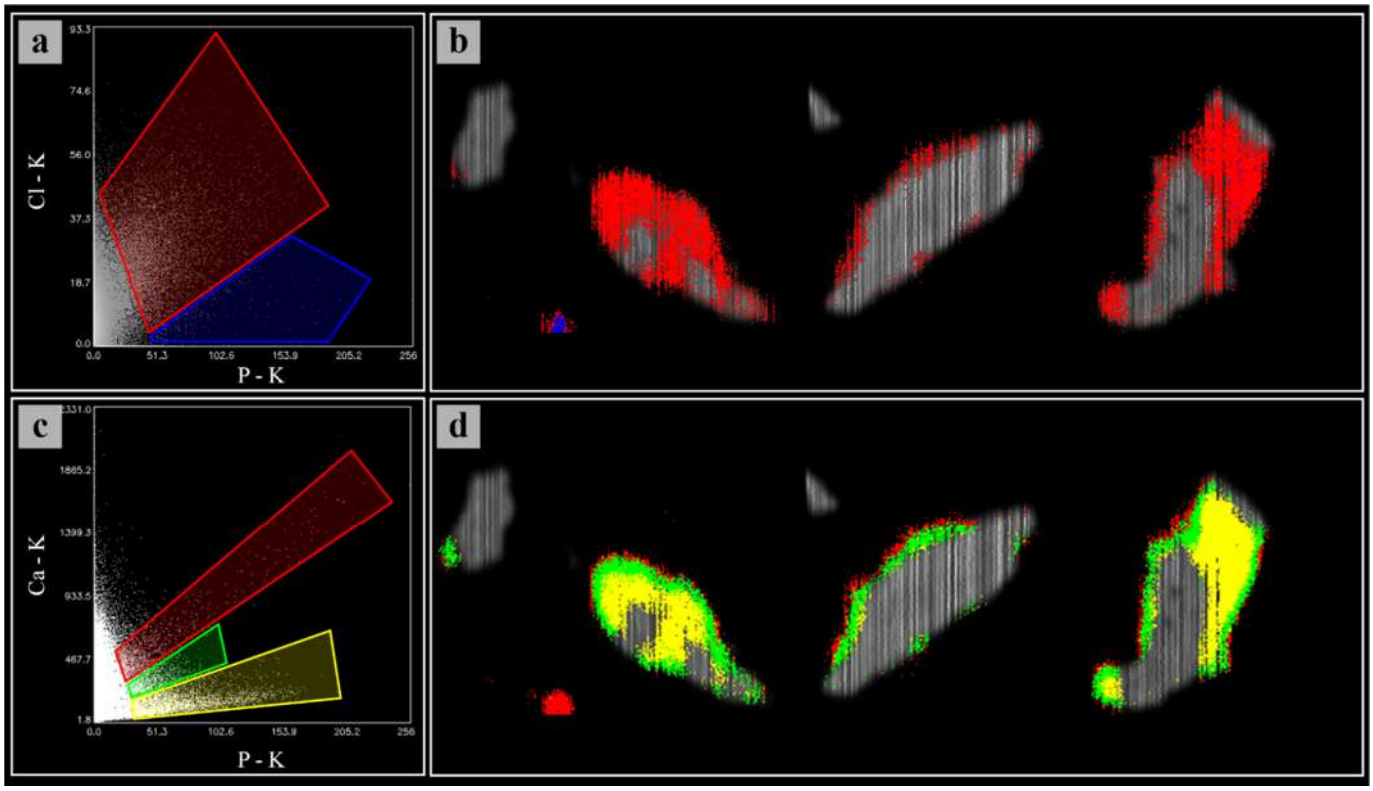

Figure 3. (**a**) Cl (K fluorescent signal) vs. P (K fluorescent signal) and (**c**) Ca (K fluorescent signal) vs. P (K fluorescent signal) scatterplots obtained using spectral μXRF deconvolution data of the three particles of Figure 2. (**b**,**d**) The three particles colored according to the different Cl–P and Ca–P correlations identified through the scatterplots (the background grey micrographs corresponding to Pb–L signals).

SEM-EDX results (Figure 4) also confirmed μXRF observations and allowed us to investigate additional features of the Pb particles and P-bearing encrustations. In the backscattered electron (BSE) image in Figure 4a (left), the darker grey regions, mainly present at the particle boundaries, indicate an average lower Z, thus the presence of lighter elements in addition to Pb. As shown by the corresponding EDX layered image (Figure 4a, right) and spectrum (Figure 4d1), this latter being relative to the white point analyses reported in the EDX image (Figure 4a, right), these low Z elements are P, Ca and Cl. In Figure 4b, which depicts a detail of the P-bearing regions, a cluster of darker grains (identified mostly as K-feldspars) ranging from a sub-micrometric scale to several micrometres in size is dispersed in a binding light grey matrix. Such matrices contain Pb, P, Ca and Cl together with Si and Al, these latter attributable to silicate fragments (region 2 and related spectrum). In Figure 4c (right), the ubiquitous occurrence of Pb, P, Ca and Cl is noticed in a compact region (spectrum d3) and within an aggregate-like structure, as well as in Figure 4b. In both Figure 4b,c, inner portions show almost only the presence of Pb (spectrum d4).

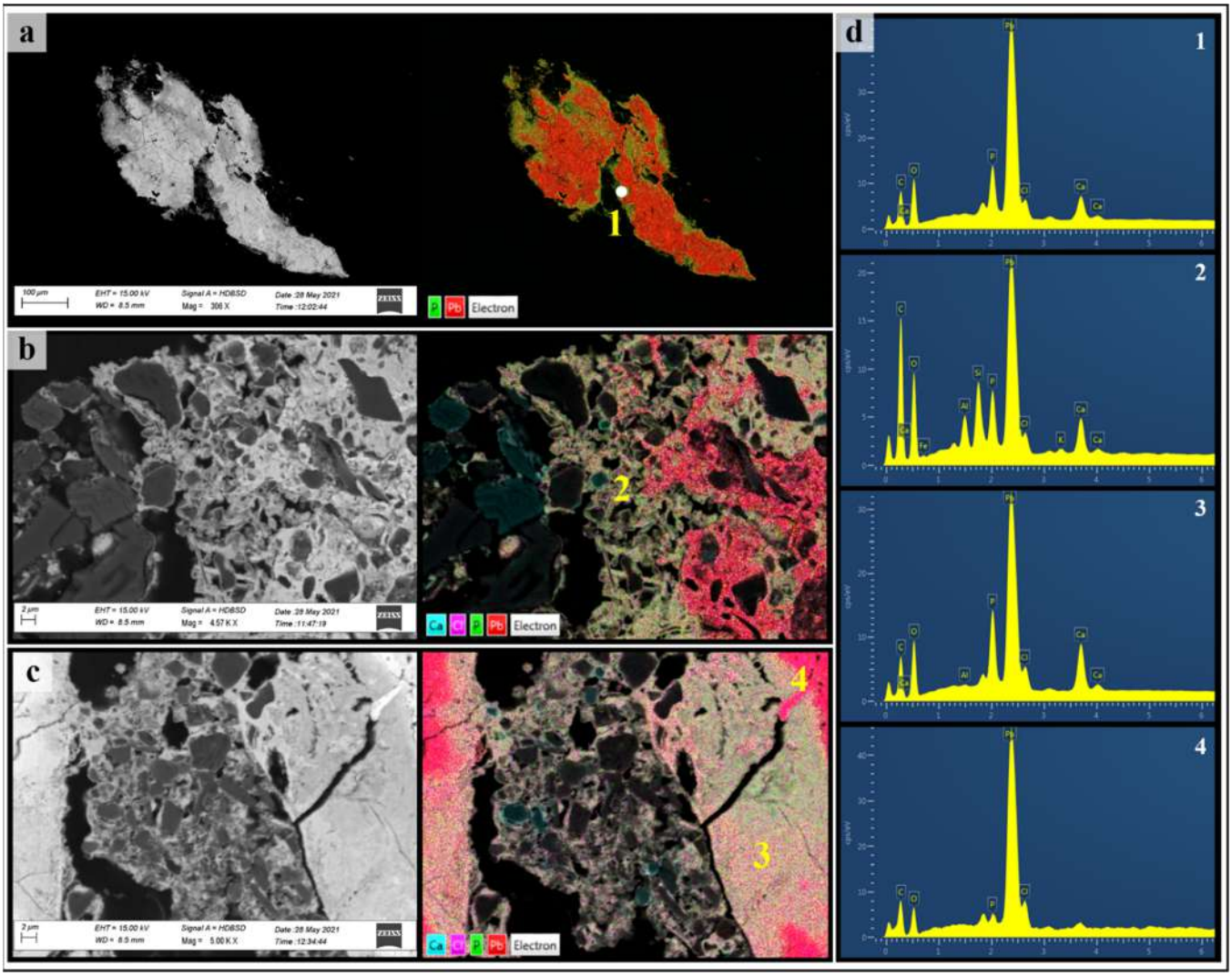

Figure 4. (**Left panel**) BSE micrographs of a Pb-containing particle. (**b**,**c**) Higher magnification details of the weathering crust of the particle shown in (**a**). (**Middle panel**) EDX layered images. (**d**, **right panel**) EDX spectra of the points (white in (**a**)) and/or regions (yellow numbers in (**b**,**c**)) indicated within the middle panel: (1) typical EDX spectrum of the P-bearing coating at particle boundaries; (2) Pb–Ca phosphates matrix in a silicate environment forming an aggregate-like structure; (3) compact Pb and Ca phosphate solid solution; (4) metallic or weakly weathered Pb.

The μXRF and SEM-EDX results described so far suggest that a weathering shell formed over time around the metallic slivers arising from the past firing range activities. Such shells consist, perhaps, of a mixture of Ca phosphate and Pb orthophosphate species, among which it has been possible to distinguish chloropyromorphite. Previous studies demonstrated that Pb stabilization as pyromorphite occurs through an intermediate Pb and Ca solid solution upon hydroxyapatite (HA) dissolution. Such an intermediate phase ($Pb_{(10-x)}Ca_x(PO_4)_6(OH)_2$–PbCaHA–) transforms into pyromorphite over time through Ca^{2+} exchange by Pb^{2+} [37–39]. In the studied slivers (Figures 2 and 3), the different correlations found between P–Pb and Ca–P seem to suggest a layering within the weathering crust, the lower Ca signal intensity indicating higher rates of Pb^{2+} substitution in the inner layers and hence a higher presence of pyromorphite. The external layers, which feature the highest Ca–P and P–Pb correlations, suggest early stages of PbCaHA formation. These sliver coatings can be further considered rather stable under the soil pH conditions. Indeed, the pH value of 7.4 measured in the polluted soil (Table 1) falls well within the pH range 3–11 in which chloropyromorphite has been found to be the most stable Pb species [36].

It could be argued that neutral to sub-alkaline pHs are yet inhibitory for pyromorphite formation due to the reduced solubility of P, which lowers both the kinetics and rate of Pb stabilization [40]. Conversely, more acidic conditions and hence soluble orthophosphate ions are required to react with Pb and precipitate pyromorphite [41]. However, a high amount of available P was measured in the soil (Table 1), and soil micro-XRF mapping also confirmed a high occurrence of P, either correlated with Ca or not: such P could have contributed to pyromorphite formation and, consequently, to Pb stabilization. Among the most common P forms in soil, apatite and phosphate rock are quite insoluble at neutral pHs. By contrast, P fertilizers, such as monocalcium and dicalcium phosphate ($Ca(H_2PO_4)_2$ and $CaHPO_4$, respectively), decrease soil pH upon dissolution, increasing the solubility of both P and Pb [40]. Based on these observations, it can be hypothesized that in the studied soil, which was used for agriculture after being dismissed as a shooting range, stabilization processes were triggered by soil phosphatic fertilization. The temporary soil acidification would have favoured pyromorphite precipitation at the fragment surfaces, thus protecting metallic Pb from further weathering processes and, at the same time, strongly limiting the possible mobilization of this hazardous element. Indeed, despite in alkaline and sub-alkaline conditions, the most commonly weathering phases of Pb bullet residues found in shooting ranges are lead carbonates and oxides (e.g., cerussite and litharge) [40], other previous studies showed the natural formation of pyromorphite in Pb-rich soils with high concentrations of available phosphates [42,43].

3.3. Bioassays with E. andrei

Considering the similarity of the physicochemical characteristics of S1 and S2 soils (Table 1), it may be hypothesized that the earthworm testing results could be only minimally influenced by the different soil properties (mainly the OM and carbonate content). In addition, the pH values of S1 and S2 (7.8 and 7.4, respectively) allow us to exclude pH-shock effects for earthworms, since they prefer circumneutral soils, even if *E. andrei* could also tolerate acidic conditions [44].

All earthworms survived after the 28-day exposure period, evidencing no acute toxicity effects, as previously experienced by other authors for similar background concentrations [5]. Moreover, the average weight of the earthworms increased after 28 days to a similar extent in both S1 and S2 mesocosms (*t*-test, $p < 0.05$). On the other hand, earthworms introduced into the polluted mesocosm accumulated significantly higher amounts of Pb in tissues and coelom fluid than the control ($p < 0.01$). Morgan and Morgan [45] found a positive correlation between Pb tissues and soil concentrations, different to other potentially toxic metals, such as Cu, Zn and Cd, whose tissue concentrations decreased proportionally as their soil concentrations increased. However, differently from these elements, Pb concentrations in earthworm tissues were generally below the soil Pb concentration, due to the higher retention of Pb by organic and inorganic soil components [46]. Even if the Pb tissue concentration of earthworms grown in S2 exceeds by ten times that of animals grown in the control soil, the bioconcentration factor (BF) obtained for S2 is very low (Table 2). Indeed, in a comprehensive study on Pb uptake in earthworms exposed to Pb-polluted soil, Langdon et al. reported a Pb tissue concentration of 266, 406 and 637 mg kg^{-1} (with corresponding BFs of 0.27, 0.14 and 0.16) for *E. andrei* exposed to 1000, 3000 and 4000 mg Pb kg^{-1}, respectively [5]. Based on these findings, an average uptake of approximately 300 mg Pb kg^{-1} in earthworm tissues exposed to S2 (1575 mg Pb kg^{-1}) should be expected, but it was only 95 mg kg^{-1} (Table 2). However, in the OECD-style experiments carried out by Langdon et al., Pb mesocosm contamination was obtained by artificially spiking the testing soils with aqueous solutions of $Pb(NO_3)_2$: this would imply higher Pb availability (and hence possibly higher Pb accumulation rates) than in field-collected soils, in which Pb can be already at least partly stabilized through complexation or adsorption to soil components (therefore less bioaccesible). Nonetheless, even by applying the regression equation proposed by Morgan and Morgan (e.g., $\log_{10}Pb_{worm} = -1.073 + 1.042 \log_{10}Pb_{soil}$), who instead worked with field-collected soils [45], the Pb uptake should be at least two times higher than our

experimental data. The value found for the control soil (11 mg kg^{-1}) is instead consistent with Langdon's results and explainable as the normal trace amount of Pb in the organisms.

Table 2. Results of bioassays with *E. andrei* in the unpolluted (S1) and polluted (S2) soils. Ecotoxicology data (mean value ± standard deviation, n = 5) with different letters in the column are statistically different according to *t*-testing ($p < 0.05$).

	Pb Concentration in Soil mg kg^{-1}	Mortality	Mean Earthworm Weight g		Pb Mean Earthworm Tissue Concentration mg kg^{-1}	Bioconcentration Factor	Pb Mean Earthworm Fluid Concentration µg L^{-1}
			Day 0	Day 28			
S1	17	0	0.36 ± 0.04 ns	0.43 ± 0.04 ns	11.1 ± 2.2 b	-	251.8 ± 55.4 b
S2	1575	0	0.35 ± 0.06 ns	0.44 ± 0.07 ns	94.9 ± 19.8 a	0.06	794.4 ± 232.2 a

ns: Not significant.

Total PTE concentration in coelom fluid has been proposed in previous studies as a bioavailability indicator [30,31,47]. Differently from the determination of total concentration in tissues, PTE quantification in fluids is not affected by possible soil residues entrapped in the gut [48]; furthermore, it is a less laborious and time-consuming procedure, and it is unnecessary to kill the animals. Looking at our results (Table 2), the increase of Pb in coelom fluid would suggest some metal sequestration mechanisms occurring within the chloragogenous tissue, which surrounds the earthworm gut epithelium, by means of metal-binding metal-inducible cysteine-rich metalloproteins, namely, metallothioneins (MTs) [49]. Albeit Pb is not recognized as a MT-inducer [50], it was detected together with Cd and Zn in the chloragogenous tissue of earthworms collected from an abandoned Zn–Pb mine in Draethen (UK), by means of proton-induced X-ray emission analysis (PIXE) [51]. In such work, Morgan et al. evidenced the primary role of Cd (and much less of Zn) in inducing MT expression in earthworms living in heavily polluted soil. This would match the possible scenario of the firing soil studied in this work and could probably explain the Pb accumulation in coelom fluids. Indeed, besides Pb, high levels of Cd, Sb and Zn (which are elements related to the past firing activity) have been detected in S2 soil (Table 1) and could have worked as MT inducers, thus favouring Pb binding, also.

Overall, the results of earthworm tests seem to depict a very limited bioavailability for soil Pb. On the one hand, neither mortality nor weight decrease was observed; rather earthworms grew over the 28-day experimental period. On the other hand, Pb bioconcentration in tissues was lower than reported in the literature for similar soil Pb concentrations, whilst a relevant amount of Pb in the coelom fluids suggested a metal-induced metal-sequestration mechanism. Such findings appear in accordance with the results of the soil characterization and microanalyses, which showed a negligible NH_4NO_3-extractable Pb fraction (Table 1) and predominant Pb stabilization by phosphates. Indeed, significant correlations between promptly bioavailable metal fractions in soils (including Pb) and their bioconcentration in earthworms have been indicated in previous works [52]. In addition, the high amount of OM in S2 (Table 1) may have contributed to limiting Pb bioavailability. At the same time, the formation of pyromorphite makes Pb inaccessible in the gastrointestinal tract, since these phases remain insoluble even after ingestion [2]. Formation of pyromorphite may also occur inside the intestine in the presence of phosphate, thanks to gastrointestinal acidic conditions [40]. These latter considerations would further confirm a low Pb accessibility in the studied case on the base of P availability.

4. Conclusions

The combination of soil microanalyses and earthworm bioavailability testing proposed in this study allowed us to comprehensively assess Pb occurrence and distribution in the investigated shooting range soil, suggesting a rather limited mobility and bioaccessibility of Pb. In these soils, Pb occurred as metallic slivers, which over time underwent weathering processes resulting in the formation of a phosphate superficial crust, in some cases encap-

sulating other soil materials within, such as small silicate minerals. The coexistence of Pb and Ca, combined with different ratios to P, suggested Pb^{2+} to Ca^{2+} exchange mechanisms, hence the stabilization of Pb into Pb orthophosphates. These latter were attributed to insoluble Cl pyromorphite formation due to the presence of Cl in the weathered regions of the particles. The occurrence of these processes is likely to strongly reduce Pb mobility and leachability in the studied soil. Earthworm bioassays confirmed this prevision, since exposure to the contaminated soil did not show acute toxicity effects (although not in the aims of the present study, these toxicity results can be extended to the other PTEs found in the investigated soils, i.e., Cd and Sb) nor high levels of Pb bioconcentration. Additional tests would be required to investigate chronic exposure effects and/or plant availability. Based on the overall results of this study, we believe that the approach pursued in this work could be successfully used for other polluted soils.

Author Contributions: Conceptualization, C.P., R.T. and M.S.; methodology, C.P. and I.A.; software, C.P. and I.A.; investigation, C.P., I.A., C.E.G. and N.F.; data curation, C.P.; writing—original draft preparation, C.P.; writing—review and editing, C.E.G., I.A., R.T., N.F., M.F. and M.S.; visualization, C.P.; supervision, M.S.; project administration, M.S.; funding acquisition, M.S., M.F. and R.T. All authors have read and agreed to the published version of the manuscript.

Funding: This research was supported by PRIN 2017 (Progetti di Ricerca di Rilevante Interesse Nazionale)—2017BHH84R—"Role of Soil-Plant-Microbial Interactions at Rhizosphere Level on the Biogeochemical Cycle and Fate of Contaminants in Agricultural Soils Under Phytoremediation with Biomass Crops (RIZOBIOREM)." Ignazio Allegretta was supported by a research grant for the project PON R&I "Studio del sistema suolo-pianta mediante tecniche analitiche innovative che impiegano raggi X"—Progetto AIM1809249—attività 1, linea 1.

Institutional Review Board Statement: Not applicable.

Informed Consent Statement: Not applicable.

Data Availability Statement: Data are available upon request by contacting Dr. Carlo Porfido (e-mail: carlo.porfido@uniba.it).

Acknowledgments: Micro-XRF and TXRF analyses were performed at the Micro-X-ray Lab of the University of Bari Aldo Moro (Italy).

Conflicts of Interest: The authors declare no conflict of interest.

References

1. Alloway, B.J. *Heavy Metals in Soil*; Blackie and Son Ltd.: London, UK, 1990; p. 339. [CrossRef]
2. Scheckel, K.G.; Diamond, G.L.; Burgess, M.F.; Klotzbach, J.M.; Maddaloni, M.; Miller, B.W.; Partridge, C.R.; Serda, S.M. Amending soils with phosphate as means to mitigate soil lead hazard: A critical review of the state of the science. *J. Toxicol. Environ. Health Part B* **2013**, *16*, 337–380. [CrossRef] [PubMed]
3. Antonovics, J.; Bradshaw, A.; Turner, R. Heavy metal tolerance in plants. In *Advances in Ecological Research*; Academic Press: Cambridge, MA, USA, 1971; Volume 7, pp. 1–85. [CrossRef]
4. Česynaitė, J.; Praspaliauskas, M.; Pedišius, N.; Sujetovienė, G. Biological assessment of contaminated shooting range soil using earthworm biomarkers. *Ecotoxicology* **2021**, *30*, 2024–2035. [CrossRef] [PubMed]
5. Langdon, C.J.; Hodson, M.E.; Arnold, R.E.; Black, S. Survival, Pb-uptake and behaviour of three species of earthworm in Pb treated soils determined using an OECD-style toxicity test and a soil avoidance test. *Environ. Pollut.* **2005**, *138*, 368–375. [CrossRef] [PubMed]
6. Roodbergen, M.; Klok, C.; van der Hout, A. Transfer of heavy metals in the food chain earthworm Black-tailed godwit (*Limosa limosa*): Comparison of a polluted and a reference site in The Netherlands. *Sci. Total Environ.* **2008**, *406*, 407–412. [CrossRef] [PubMed]
7. Allegretta, I.; Porfido, C.; Martin, M.; Barberis, E.; Terzano, R.; Spagnuolo, M. Characterization of As-polluted soils by laboratory X-ray-based techniques coupled with sequential extractions and electron microscopy: The case of Crocette gold mine in the Monte Rosa mining district. *Environ. Sci. Pollut. Res.* **2018**, *25*, 25080–25090. [CrossRef] [PubMed]
8. Gattullo, C.E.; D'Alessandro, C.; Allegretta, I.; Porfido, C.; Spagnuolo, M.; Terzano, R. Alkaline hydrothermal stabilization of Cr(VI) in soil using glass and aluminum from recycled municipal solid wastes. *J. Hazard. Mater.* **2018**, *344*, 381–389. [CrossRef] [PubMed]

9. Sosa, N.N.; Kulkarni, H.; Datta, S.; Beilinson, E.; Porfido, C.; Spagnuolo, M.; Zárate, M.A.; Surber, J. Occurrence and distribution of high arsenic in sediments and groundwater of the Claromecó fluvial basin, southern Pampean plain. *Sci. Total Environ.* **2019**, *695*, 133673. [CrossRef]
10. Gattullo, C.E.; Allegretta, I.; Porfido, C.; Rascio, I.; Spagnuolo, M.; Terzano, R. Assessing chromium pollution and natural stabilization processes in agricultural soils by bulk and micro X-ray analyses. *Environ. Sci. Pollut. Res.* **2020**, *27*, 22967–22979. [CrossRef] [PubMed]
11. MacLean, L.C.W.; Beauchemin, S.; Rasmussen, P.E. Lead speciation in house dust from canadian urban homes using EXAFS, Micro-XRF, and Micro-XRD. *Environ. Sci. Technol.* **2011**, *45*, 5491–5497. [CrossRef]
12. McIntosh, K.G.; Cordes, N.L.; Patterson, B.M.; Havrilla, G.J. Laboratory-based characterization of plutonium in soil particles using micro-XRF and 3D confocal XRF. *J. Anal. At. Spectrom.* **2015**, *30*, 1511–1517. [CrossRef]
13. Landrot, G.; Khaokaew, S. Determining the fate of lead (Pb) and phosphorus (P) in alkaline Pb-polluted soils amended with P and acidified using multiple synchrotron-based techniques. *J. Hazard. Mater.* **2020**, *399*, 123037. [CrossRef] [PubMed]
14. Li, Q.; Hu, X.; Hao, J.; Chen, W.; Cai, P.; Huang, Q. Characterization of Cu distribution in clay-sized soil aggregates by NanoSIMS and micro-XRF. *Chemosphere* **2020**, *249*, 126143. [CrossRef] [PubMed]
15. Weltje, L. Mixture toxicity and tissue interactions of Cd, Cu, Pb and Zn in earthworms (Oligochaeta) in laboratory and field soils: A critical evaluation of data. *Chemosphere* **1998**, *36*, 2643–2660. [CrossRef]
16. Martin, M.H.; Coughtrey, P.J. The use of terrestrial animals as monitors and indicators of environmental contamination by heavy metals. In *Biological Monitoring of Heavy Metal Pollution*; Springer: Dordrecht, The Netherlands, 1982; pp. 221–310. [CrossRef]
17. Ireland, M.P. *Heavy Metal Uptake and Tissue Distribution in Earthworms*; Springer Science and Business Media LLC: Berlin/Heidelberg, Germany, 1983; pp. 247–265.
18. Ministerial Decree. n. 46/2019. Available online: https://www.gazzettaufficiale.it/eli/id/2019/06/07/19G00052/sg (accessed on 29 September 2021).
19. Gee, G.W.; Bauder, J.W. Particle-size analysis. In *Methods of Soil Analysis. Part 1: Physical and Mineralogical Methods*, 2nd ed.; Klute, A., Ed.; American Society of Agronomy: Madison, WI, USA, 1986; pp. 383–411.
20. Slavich, P.; Petterson, G. Estimating the electrical conductivity of saturated paste extracts from 1:5 soil, water suspensions and texture. *Soil Res.* **1993**, *31*, 73–81. [CrossRef]
21. Bloom, P.R.; Meter, K.; Crum, J.R. Titration method for determination of clay-sized carbonates. *Soil Sci. Soc. Am. J.* **1985**, *49*, 1070–1073. [CrossRef]
22. Sparks, D.L.; Page, A.L.; Helmke, P.A.; Loeppert, R.H.; Soltanpour, P.N.; Tabatabai, M.A.; Johnston, C.T.; Sumner, M.E. *Methods of Soil Analysis: Part 3 Chemical Methods 5.3*, 1st ed.; Soil Science Society of America Book Series 5; Soil Science Society of America, Inc.; American Society of Agronomy, Inc.: Madison, WI, USA, 1996; p. 1390. [CrossRef]
23. Duri, L.G.; Visconti, D.; Fiorentino, N.; Adamo, P.; Fagnano, M.; Caporale, A.G. Health risk assessment in agricultural soil potentially contaminated by geogenic Thallium: Influence of plant species on metal mobility in soil-plant system. *Agronomy* **2020**, *10*, 890. [CrossRef]
24. BBodSchV. Bundes-Bodenschutz- und Altlastenverordnung (BBodSchV) vom 12. Juli 1999. Bundesgesetzblatt I 1999, 1554 (English Version) [Federal Soil Protection and Contaminated Sites Ordinance, Dated 12 July 1999]. 1999. Available online: https://www.elaw.org/es/content/germany-federal-soil-protection-and-contaminated-sites-ordinance-bbodschv-12-july-1999 (accessed on 29 September 2021).
25. Gupta, S.; Vollmer, M.; Krebs, R. The importance of mobile, mobilisable and pseudo total heavy metal fractions in soil for three-level risk assessment and risk management. *Sci. Total Environ.* **1996**, *178*, 11–20. [CrossRef]
26. Kingston, H.M.; Haswell, S.J. *Microwave-Enhanced Chemistry: Fundamentals, Sample Preparation, and Applications*; American Chemical Society: Washington, DC, USA, 1997.
27. Solé, V.; Papillon, E.; Cotte, M.; Walter, P.; Susini, J. A multiplatform code for the analysis of energy-dispersive X-ray fluorescence spectra. *Spectrochim. Acta Part B At. Spectrosc.* **2007**, *62*, 63–68. [CrossRef]
28. Alfeld, M.; Janssens, K. Strategies for processing mega-pixel X-ray fluorescence hyperspectral data: A case study on a version of Caravaggio's painting Supper at Emmaus. *J. Anal. At. Spectrom.* **2015**, *30*, 777–789. [CrossRef]
29. OECD. Guideline for Testing of Chemicals no. 207. Earthworm, Acute Toxicity Test. 1984. Available online: https://www.oecd.org/chemicalsafety/risk-assessment/1948293.pdf (accessed on 3 January 2021).
30. Allegretta, I.; Porfido, C.; Panzarino, O.; Fontanella, M.C.; Beone, G.M.; Spagnuolo, M.; Terzano, R. Determination of as concentration in earthworm coelomic fluid extracts by total-reflection X-ray fluorescence spectrometry. *Spectrochim. Acta Part B At. Spectrosc.* **2017**, *130*, 21–25. [CrossRef]
31. Porfido, C.; Allegretta, I.; Panzarino, O.; Laforce, B.; Vekemans, B.; Vincze, L.; de Lillo, E.; Terzano, R.; Spagnuolo, M. Correlations between as in earthworms' coelomic fluid and as bioavailability in highly polluted soils as revealed by combined laboratory X-ray techniques. *Environ. Sci. Technol.* **2019**, *53*, 10961–10968. [CrossRef] [PubMed]
32. USDA Soil Survey Staff, Natural Resources Conservation Service, United States Department of Agriculture. Official Soil Series Descriptions. Available online: https://www.nrcs.usda.gov/wps/portal/nrcs/detail/soils/survey/geo/?cid=nrcs142p2_053587 (accessed on 3 January 2021).
33. Jowett, M.; Price, H.I. Solubilities of the phosphates of lead. *Trans. Faraday Soc.* **1932**, *28*, 668–681. [CrossRef]
34. Lindsay, W.L. *Chemical Equilibria in Soils*; John Wiley and Sons: Hoboken, NJ, USA, 1979.

35. Scheckel, K.G.; Ryan, J.A. Effects of aging and pH on dissolution Kinetics and stability of Chloropyromorphite. *Environ. Sci. Technol.* **2002**, *36*, 2198–2204. [CrossRef] [PubMed]
36. Nriagu, J.O. Lead orthophosphates—IV Formation and stability in the environment. *Geochim. Cosmochim. Acta* **1974**, *38*, 887–898. [CrossRef]
37. Mavropoulos, E.; Rossi, A.M.; Costa, A.M.; Perez, C.A.C.; Moreira, J.C.; Saldanha, M. Studies on the mechanisms of lead immobilization by hydroxyapatite. *Environ. Sci. Technol.* **2002**, *36*, 1625–1629. [CrossRef]
38. Mavropoulos, E.; Rocha, N.C.; Moreira, J.C.; Rossi, A.M.; Soares, G.A. Characterization of phase evolution during lead immobilization by synthetic hydroxyapatite. *Mater. Charact.* **2004**, *53*, 71–78. [CrossRef]
39. Miretzky, P.; Fernandez-Cirelli, A. Phosphates for Pb immobilization in soils: A review. *Environ. Chem. Lett.* **2008**, *6*, 121–133. [CrossRef]
40. Chrysochoou, M.; Dermatas, D.; Grubb, D.G. Phosphate application to firing range soils for Pb immobilization: The unclear role of phosphate. *J. Hazard. Mater.* **2007**, *144*, 1–14. [CrossRef] [PubMed]
41. Porter, S.K.; Scheckel, K.G.; Impellitteri, C.A.; Ryan, J.A. Toxic metals in the environment: Thermodynamic considerations for possible immobilization strategies for Pb, Cd, As, and Hg. *Crit. Rev. Environ. Sci. Technol.* **2004**, *34*, 495–604. [CrossRef]
42. Cao, X.; Ma, L.Q.; Chen, M.; Hardison, D.W.; Harris, W.G. Lead transformation and distribution in the soils of shooting ranges in Florida, USA. *Sci. Total Environ.* **2003**, *307*, 179–189. [CrossRef]
43. Cotter-Howells, J. Lead phosphate formation in soils. *Environ. Pollut.* **1996**, *93*, 9–16. [CrossRef]
44. Edwards, C.A.; Bohlen, P.J. *Biology and Ecology of Earthworms*, 3rd ed.; Chapman & Hall: London, UK, 1996.
45. Morgan, J.; Morgan, A. Earthworms as biological monitors of cadmium, copper, lead and zinc in metalliferous soils. *Environ. Pollut.* **1988**, *54*, 123–138. [CrossRef]
46. Zimdahl, R.L.; Skogerboe, R.K. Behavior of lead in soil. *Environ. Sci. Technol.* **1977**, *11*, 1202–1207. [CrossRef]
47. Tan, Q.-G.; Ke, C.; Wang, W.-X. Rapid Assessments of metal bioavailability in marine sediments using coelomic fluid of sipunculan worms. *Environ. Sci. Technol.* **2013**, *47*, 7499–7505. [CrossRef]
48. Chapman, P.M. Effects of gut sediment contents on measurements of metal levels in benthic invertebrates—A Cautionary Note. *Bull. Environ. Contam. Toxicol.* **1985**, *35*, 345–347. [CrossRef]
49. Adamowicz, A. Morphology and ultrastructure of the earthworm *Dendrobaena veneta* (Lumbricidae) coelomocytes. *Tissue Cell* **2005**, *37*, 125–133. [CrossRef]
50. Kägi, J.H. Overview of metallothionein. *Methods Enzymol.* **1991**, *205*, 613–626. [CrossRef]
51. Morgan, A.; Stürzenbaum, S.; Winters, C.; Grime, G.; Aziz, N.A.A.; Kille, P. Differential metallothionein expression in earthworm (*Lumbricus rubellus*) tissues. *Ecotoxicol. Environ. Saf.* **2004**, *57*, 11–19. [CrossRef]
52. Dai, J.; Becquer, T.; Rouiller, J.H.; Reversat, G.; Bernhard-Reversat, F.; Nahmani, J.; Lavelle, P. Heavy metal accumulation by two earthworm species and its relationship to total and DTPA-extractable metals in soils. *Soil Biol. Biochem.* **2003**, *36*, 91–98. [CrossRef]